

# V노치 및 예리한 균열을 갖는 $N$ 다변형 단면 입체 실린더의 3차원 진동해석

## Three-Dimensional Vibration Analysis of Solid Cylinders of $N$ -Sided Polygonal Cross-Section Having V-notches or Sharp Cracks

김 주 우<sup>1)</sup>

Kim, Joo Woo

**요 약**: 본 연구는 V노치 또는 예리한 균열이 존재하는  $N$  다변형 단면 입체 실린더에 대한 새로운 3차원 진동 데이터를 제시한다. 본 논문에서는 수학적으로 완전한 대수삼각다항식과 V노치 선단을 따라 존재하는 3차원 응력특이도를 명확히 다루는 허용예지함수와 함께 Ritz방법이 적용된다. 응력특이도를 포함하는 다변형 입체 실린더의 정확한 고유진동수 및 모드형상을 얻기 위해서는 예지함수가 필요하다는 것이 수렴도 분석을 통하여 입증된다.

**ABSTRACT**: In this paper, new three-dimensional vibration data for the solid cylinders of the  $N$ -sided polygonal cross-section with V-notches or sharp cracks are presented, and a Ritz procedure is employed, which incorporates a mathematically complete set of algebraic-trigonometric polynomials in conjunction with an admissible set of edge functions that explicitly model the tri-axial stress singularities that exist along a terminus edge of the V-notch. Convergence studies demonstrate the necessity of adding the edge functions to achieve the accurate frequencies and mode shapes of  $N$ -sided polygonal cylindrical solids with stress singularities.

**핵심용어**: Ritz법, 다변형 입체 실린더, 3차원 탄성론, 자유진동, 3차원 응력특이도, 예지함수, 고유진동수

**KEYWORDS**: Ritz method, Polygonal cylindrical solid, Three-dimensional elasticity theory, Free vibration, Three-dimensional stress singularities, Edge function, Natural frequency

### 1. INTRODUCTION

Solid cylinders of polygonal cross-section can be commonly seen in civil, aerospace and ocean engineering systems. The computational difficulties in three-dimensional modeling of polygonal cylinders have led to the development of simple refined beam theories (Timoshenko, 1921a; Timoshenko, 1921b). The three-dimensional analyses place none of the kinematic constraints of the one- or two-dimensional theories. Usually, effective solutions to the three-dimensional dynamic problems of elastic bodies are very difficult to obtain. Therefore, despite the practical needs for three-dimensional vibration solutions to this engineering problems, very little has been done in the associated

literature of cylindrical elastic solids. Specifically no previously published data is known to exist for solid cylinders of polygonal cross-section with V-notches or sharp cracks. Understanding the vibration characteristics require three-dimensional prediction procedure, which is based upon three-dimensional theory of elasticity. A three-dimensional analysis places none of the kinematic constraints of the two-dimensional theories.

One effort was performed by Kim, *et al.* (2001), who presented the vibration data of three-dimensional parallelepipeds by considering the stress singularities using the Ritz procedure. Recently, the natural frequencies of V-notched or cracked hexagonal plates are offered using classically thin plate theory(Kim, *et al.*, 2006) and Mindlin plate theory (Kim and Jung, 2007).

1) 교신저자, 세명대학교 건축공학과 교수, 공학박사  
(Tel. 043-649-1329, Fax. 043-649-1755, E-mail: jw\_kim@semyung.ac.kr)

본 논문에 대한 토의를 2010년 2월 28일까지 학회로 보내주시면 토의 회답을 게재하겠습니다.

Using the Ritz method the free vibration data of complete solid cylinders with polygonal cross-sections are reported by Liew, *et al.* (1997).

The present work examines the solid cylinders of  $N$ -sided polygonal cross-section having V-notches and sharp radial cracks, for which no previously published vibration frequencies is known to exist. The relative depth of the V-notch is defined as  $1 - c/a$  and the notch angle is defined as  $360^\circ - \alpha$  (Fig. 1). For a very small notch angle (one degree or less), the notch may be regarded as a radial crack.

In this study a single-field Ritz procedure is employed, which incorporates a complete set of admissible algebraic-trigonometric polynomials in conjunction with an admissible set of edge functions that explicitly model the three-dimensional stress singularities which exist along a reentrant vertex (i.e.,  $\alpha > 180^\circ$ ) of the V-notch. The first set of polynomials guarantees convergence to exact frequencies as sufficient terms are retained. The second set of edge functions substantially accelerates the convergence of frequencies, which is demonstrated through extensive convergence studies herein. Accurate (five significant figure) frequencies are presented for  $N$ -sided polygonal cylindrical solids having various notch angles.

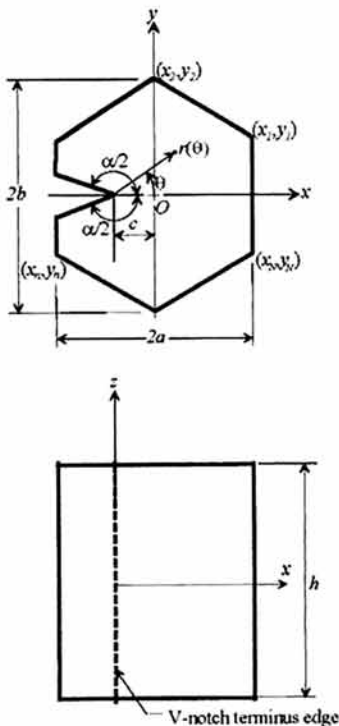


Fig. 1. An elastic solid cylinder of  $N$ -sided polygonal cross-section with a V-notch

## 2. METHOD OF ANALYSIS

Consider in Fig. 1 a completely free, isotropic elastic solid polygonal cylinder with height of  $h$  and cylindrical coordinates  $(r, \theta, z)$  originating at the terminus of the V-notch on middle surface. The location of the V-notch terminus is defined by the horizontal distance  $c$ . For the three-dimensional Ritz approach, the vibratory displacement functions are assumed as

$$u_r(r, \theta, z, t) = U_r(r, \theta, z) \sin \omega t, \quad (1a)$$

$$v_\theta(r, \theta, z, t) = V_\theta(r, \theta, z) \sin \omega t, \quad (1b)$$

$$w_z(r, \theta, z, t) = W_z(r, \theta, z) \sin \omega t, \quad (1c)$$

where the  $U_r$  and  $V_\theta$  are in-plane displacement amplitudes in  $r$  and  $\theta$  directions, respectively and  $W_z$  is transverse displacement amplitude, and  $\omega$  and  $t$  denote the circular frequency of vibration and time, respectively.

The maximum strain energy during a vibratory cycle is represented by

$$V_{\max} = \frac{1}{2} \iiint \left\{ (K + 2G) \left[ \left( \frac{\partial U_r}{\partial r} \right)^2 + \left( \frac{\partial W_z}{\partial z} \right)^2 \right. \right. \\ \left. \left. + \frac{1}{r^2} \left( U_r + \frac{\partial V_\theta}{\partial \theta} \right)^2 \right] + 2K \left[ \frac{\partial U_r}{\partial r} \frac{\partial W_z}{\partial z} + \frac{1}{r} \left( U_r + \frac{\partial V_\theta}{\partial \theta} \right) \right. \right. \\ \left. \left. + \left( \frac{\partial U_r}{\partial r} + \frac{\partial W_z}{\partial z} \right) \right] + \frac{G}{r^2} \left[ \left( \frac{\partial U_r}{\partial \theta} + r \frac{\partial V_\theta}{\partial r} - V_\theta \right)^2 \right. \right. \\ \left. \left. + \left( r \frac{\partial V_\theta}{\partial z} + \frac{\partial W_z}{\partial \theta} \right)^2 \right] + G \left( \frac{\partial U_r}{\partial z} + \frac{\partial W_z}{\partial r} \right)^2 \right\} r dr d\theta dz. \quad (2)$$

In Eq. (2),  $K$  and  $G$  are the Lamé constants

$$K = \frac{\nu E}{(1 + \nu)(1 - 2\nu)}, \quad G = \frac{E}{2(1 - 2\nu)},$$

where  $E$  is Young's modulus, and  $\nu$  is Poisson's ratio.

The maximum kinetic energy is

$$T_{\max} = \frac{\rho \omega^2}{2} \iiint (U_r^2 + V_\theta^2 + W_z^2) r dr d\theta dz. \quad (3)$$

in which  $\rho$  is the mass per unit volume. In Eqs. (2) and (3), the limit of integrations is defined as  $r(\theta)$ , describing the hexagonal circumferential boundary:

$$r(\theta) = \frac{|y_n - x_n \tan \eta_n|}{\sin \theta - \tan \eta_n \cos \theta} \quad (-\pi \leq \theta \leq \pi), \quad (4a)$$

where number of sides  $n = 1, 2, \dots, N$  (for hexagon,  $N = 6$  as shown in Fig. 1). The above equation can be applied to all range of  $\theta$  for hexagon except following cases:

$$r(\theta) = -\frac{a-c}{\cos \theta} \quad \left(\theta_{\frac{N}{2}} \leq \theta \leq \theta_{\frac{N}{2}+1}\right), \quad (4b)$$

$$r(\theta) = \frac{a+c}{\cos \theta} \quad (\theta_N \leq \theta \leq \theta_1). \quad (4c)$$

In the Eq. (4a),

$$\begin{cases} \eta_1 = \beta + \frac{\pi}{2} \\ \eta_n = \eta_{n-1} + \beta \end{cases} \quad (4d)$$

$$\begin{cases} x_1 = a + c \\ x_n = x_{n-1} + L \cos \eta_{n-1} \end{cases} \quad (4e)$$

$$\begin{cases} y_1 = \frac{L}{2} - d \\ y_n = y_{n-1} + L \sin \eta_{n-1} \end{cases} \quad (4f)$$

in which  $n = 1, 2, \dots, N$  and

$$\beta = \frac{2\pi}{N}, \quad L = 2a \tan \frac{\beta}{2}. \quad (4g)$$

The required area integral in the dynamical energy Eqs. (2) and (3) can be performed numerically.

In the present three-dimensional Ritz analysis, displacement trial functions are assumed as the sum of two finite sets

$$U_r = U_r^p + U_r^c, \quad V_\theta = V_\theta^p + V_\theta^c, \quad W_z = W_z^p + W_z^c. \quad (5)$$

where  $U_r^p$ ,  $V_\theta^p$ , and  $W_z^p$  are the admissible and

mathematically complete set of algebraic-trigonometric polynomials and  $U_r^c$ ,  $V_\theta^c$ , and  $W_z^c$  are admissible edge functions, which account for singular stress behavior along the terminus edge of the V-notch (see Fig. 1). The chosen algebraic-trigonometric polynomial functions are written as

$$U_r^p(r, \theta, z) = \sum_{i=2,4j=0.2,4k=0}^{I_1} \sum_i^i \sum_{K_1}^{K_1} A_{ijk} r^{i-1} \cos j\theta z^k + \sum_{i=1,3,5j=1,3,5k=0}^{I_2} \sum_i^i \sum_{K_2}^{K_2} A_{ijk} r^{i-1} \cos j\theta z^k, \quad (6a)$$

$$V_\theta^p(r, \theta, z) = \sum_{i=2,4j=0.2,4k=0}^{I_3} \sum_i^i \sum_{K_3}^{K_3} B_{ijk} r^{i-1} \sin j\theta z^k + \sum_{i=1,3,5j=1,3,5k=0}^{I_4} \sum_i^i \sum_{K_4}^{K_4} B_{ijk} r^{i-1} \sin j\theta z^k, \quad (6b)$$

$$W_z^p(r, \theta, z) = \sum_{i=2,4j=0.2,4k=0}^{I_5} \sum_i^i \sum_{K_5}^{K_5} C_{ijk} r^i \cos j\theta z^k + \sum_{i=3,5j=1,3,5k=0}^{I_6} \sum_i^i \sum_{K_6}^{K_6} C_{ijk} r^i \cos j\theta z^k \quad (6c)$$

for the symmetric vibration modes when  $d = 0$  in Fig. 1. In Eqs. (6),  $A_{ijk} - C_{ijk}$  are undetermined coefficients, and the values of  $i$  are specially chosen to avoid unacceptable stress singularities at  $r = 0$  and yet preserve the mathematical completeness of the resulting series. Hence convergence to the exact frequency solutions is guaranteed as sufficient solution sizes of this series are retained in the present Ritz procedure.

The displacement polynomial functions in Eqs. (5) and (6) should theoretically yield accurate frequencies even for the polygons having stress singularities. However, when a large size of polynomials is utilized, numerical ill-conditioning becomes an obstacle and prohibits one from achieving accurate solutions. This problem is alleviated by augmentation of the displacement polynomial trial set with admissible edge functions, which introduce the proper three-dimensional singular vibratory stresses along the terminus edge of a V-notch or sharp radial crack.

The set of edge function is taken as

$$U_r^e = \sum_{m=1}^{M_1} \sum_{n=0}^{N_1} G_{mn} r^{\lambda_m} [-r_{1m} \eta_m \cos(\lambda_m + 1)\theta + \cos(\lambda_m - \theta)] z^n, \quad (7a)$$

$$V_\theta^e = \sum_{m=1}^{M_2} \sum_{n=0}^{N_2} G_{mn} r^{\lambda_m} [-r_{2m} \eta_m \sin(\lambda_m + 1)\theta - \zeta_m \sin(\lambda_m - 1)\theta] z^n, \quad (7b)$$

$$W_z^e = \sum_{m=1}^{M_3} \sum_{n=0}^{N_3} H_{mn} r^{\bar{\lambda}_m} (\cos \bar{\lambda}_m \theta) z^n, \quad (7c)$$

in which

$$\gamma_{1m} = \frac{\cos(\lambda_m - 1)\alpha/2}{\cos(\lambda_m + 1)\alpha/2}, \quad \gamma_{2m} = \frac{\cos(\lambda_m - 1)\alpha/2}{\cos(\lambda_m - 1)\alpha/2} \quad (7d)$$

$$\eta_m = \frac{\lambda_m + 1}{\lambda_m - 3 + 4\nu}, \quad \zeta_m = \frac{\lambda_m + 3 - 4\nu}{\lambda_m - 3 + 4\nu} \quad (7e)$$

for the symmetric vibration modes. In Eqs. (7),  $G_{mn}$  and  $H_{mn}$  are arbitrary coefficients again and  $\lambda_m$  and  $\bar{\lambda}_m$  are the roots of the characteristic equations

$$\sin \lambda_m \alpha = -\lambda_m \sin \alpha \quad \sin(\bar{\lambda}_m + 1)\alpha/2 \quad (8)$$

Similarly, for the antisymmetric modes, algebraic-trigonometric polynomials and the corresponding edge functions are analogous to those defined for the symmetric ones in Eqs. (6) and (7), except the cosine functions are changed to sine functions, or vice versa, and the corresponding characteristic equations are

$$\sin \lambda_m \alpha = \lambda_m \sin \alpha \quad \cos(\bar{\lambda}_m + 1)\alpha/2 \quad (9)$$

Some of the  $\lambda_m$  obtained from Eqs. (8) and (9) may be complex numbers, and thus results in complex edge functions. In such cases, both the real and imaginary parts are used as independent functions in the present Ritz procedure.

The free vibration problem is solved by substituting Eqs. (5)-(7) into Eqs. (2) and (3) and employing the frequency equations of the Ritz method. For the symmetric modes, for instance, these are:

$$\frac{\partial(V_{\max} - T_{\max})}{\partial A_{ijk}} = 0, \quad \frac{\partial(V_{\max} - T_{\max})}{\partial B_{ijk}} = 0$$

$$\frac{\partial(V_{\max} - T_{\max})}{\partial C_{ijk}} = 0, \quad (10a)$$

$$\frac{\partial(V_{\max} - T_{\max})}{\partial G_{mn}} = 0, \quad \frac{\partial(V_{\max} - T_{\max})}{\partial H_{mn}} = 0 \quad (10b)$$

Eqs. (10) result in a set of linear homogeneous algebraic equations in terms of the undetermined coefficients  $A_{ijk}$ ,  $B_{ijk}$ ,  $C_{ijk}$ ,  $G_{mn}$ , and  $H_{mn}$ . The vanishing determinant of this equation yields a set of eigenvalues (natural frequencies) expressed in terms of the non-dimensional frequency parameters. Eigenvectors (i.e., mode shapes) involving the coefficients  $A_{ijk}$ ,  $B_{ijk}$ ,  $C_{ijk}$ ,  $G_{mn}$ , and  $H_{mn}$  may be determined in the usual manner by substituting the eigenvalues back into the homogeneous equations. The non-dimensional frequency parameter  $\Lambda$  is related to the natural angular frequency  $\omega$  by

$$\Lambda = \frac{\omega l^2}{h} \sqrt{\rho/E}, \quad (11)$$

in which  $l = 2b$  (see Fig. 1).

### 3. CONVERGENCE STUDIES

The three-dimensional Ritz formulation described in the previous section is now employed to obtain reasonably convergent frequency solutions as sufficient numbers of algebraic-trigonometric polynomials and three-dimensional edge functions are utilized. In all calculations, the Poisson's ratio  $\nu$  has been set to 0.3. All of the frequency calculations in this work were performed using extended precision (28 significant figure) arithmetic. According to the number of sides ( $N$ ) of the polygonal cylinders, they may be pentagonal, hexagonal, heptagonal, octagonal shaped cylinders and so on. Here, as an example for the sake of brevity, convergence studies are summarized for the completely free hexagonal cylindrical solid (i.e.,  $N=6$ ) with  $h/l = 2$  having two types of V-notches, both having

$\alpha = 355^\circ$  but different notch depths. These are: (i) a shallow notch ( $c/a = 0.75$ ) and (ii) a deep notch ( $c/a = 0.0$ ) for which the plane of symmetry in  $\theta$  is used (see Fig. 1). These examples are also described as a hexagonal cylinders with a sharp crack appropriately. The configurations of the examples are depicted in Fig. 2 along with the cases  $c/a = 0.5$  and  $c/a = -0.5$ .

Shown in Table 1 is the first six non-dimensional frequencies  $\Lambda$  for the deep notch ( $c/a = 0$ ). It should be noticed that the first six modes are rigid body modes in the three-dimensional vibration of completely free hexagonal cylindrical solids having V-notch (see Fig. 1). These rigid body frequencies, which are zero, are not shown in the table. Frequency results are obtained as  $4 \times 10$ ,  $5 \times 10$ ,  $6 \times 10$ ,  $7 \times 10$ , and  $8 \times 10$  polynomial solutions are used in conjunction with  $0$ ,  $5 \times 10$ ,  $10 \times 10$ ,  $20 \times 10$ , and  $30 \times 10$  edge function solutions for each symmetry class in  $\theta$ .

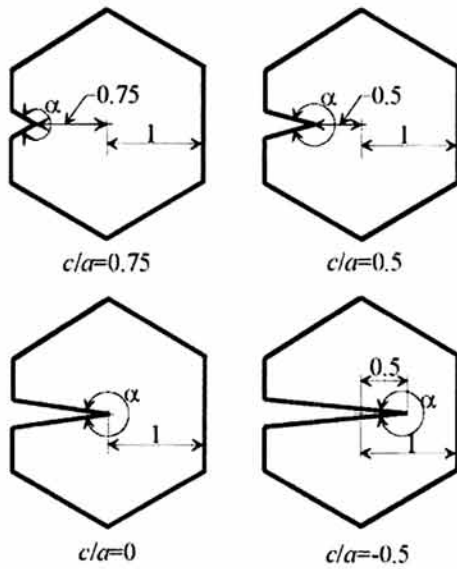


Fig 2. V-notches with various depths

In Table 1, consider the fundamental frequency mode, which is an antisymmetric one. The use of polynomial functions alone results in the upper-bound convergence to an inaccurate  $\Lambda$  value of 0.4578. The trial set consisting of the first five edge functions along with as little as  $4 \times 10$  polynomials yields an upper-bound frequency value which is much lower

(25.3 %) than the first row of  $\Lambda$  obtained using no edge functions. An examination of the next four rows of data reveals that an accurate  $\Lambda$  to five significant figures is 0.3361. Similar level of convergence rate can be seen for the higher modes.

In Table 2, frequency data for much shallower sharp notch ( $c/a = 0.75$ ) are shown. It can be seen in this table that the fundamental frequency mode is an antisymmetric mode. Compared with the previous data for the deep notch, it is seen for the shallow notch that convergence is slightly slower. Nevertheless, it can be seen in Table 2 that convergence to five significant figures is essentially achieved for the first six modes.

Table 1. Convergence of frequency parameters  $\Lambda$  for a completely free hexagonal cylindrical solid ( $N = 6$ ) having a V-notch ( $\alpha = 355^\circ$ ,  $c/a = 0$ ,  $h/l = 2$ )

Mode no. (sym. class *)	Size of edge function	Solution size of polynomials				
		$4 \times 10$	$5 \times 10$	$6 \times 10$	$7 \times 10$	$8 \times 10$
1 (A)	0	0.4589	0.4579	0.4579	0.4578	0.4578
	$5 \times 10$	0.3424	0.3381	0.3370	0.3369	0.3368
	$10 \times 10$	0.3370	0.3369	0.3368	0.3367	0.3367
	$20 \times 10$	0.3366	0.3365	0.3364	0.3364	0.3364
	$30 \times 10$	0.3363	0.3362	0.3361	0.3361	—
2 (A)	0	0.4870	0.4869	0.4752	0.4751	0.4751
	$5 \times 10$	0.4148	0.4139	0.4137	0.4136	0.4135
	$10 \times 10$	0.4139	0.4136	0.4135	0.4135	0.4134
	$20 \times 10$	0.4138	0.4135	0.4135	0.4134	0.4134
	$30 \times 10$	0.4137	0.4135	0.4134	0.4134	—
3 (S)	0	0.4562	0.4553	0.4553	0.4552	0.4552
	$5 \times 10$	0.4445	0.4436	0.4412	0.4407	0.4394
	$10 \times 10$	0.4415	0.4412	0.4410	0.4402	0.4394
	$20 \times 10$	0.4397	0.4394	0.4392	0.4392	0.4391
	$30 \times 10$	0.4396	0.4393	0.4392	0.4391	—
4 (S)	0	0.7755	0.7755	0.7755	0.7755	0.7755
	$5 \times 10$	0.4603	0.4597	0.4587	0.4585	0.4581
	$10 \times 10$	0.4588	0.4587	0.4586	0.4583	0.4581
	$20 \times 10$	0.4582	0.4581	0.4580	0.4580	0.4580
	$30 \times 10$	0.4581	0.4581	0.4580	0.4580	—
5 (S)	0	0.8869	0.8821	0.8821	0.8816	0.8816
	$5 \times 10$	0.5282	0.5262	0.5228	0.5225	0.5212
	$10 \times 10$	0.5233	0.5230	0.5225	0.5218	0.5210
	$20 \times 10$	0.5215	0.5212	0.5208	0.5208	0.5207
	$30 \times 10$	0.5213	0.5211	0.5207	0.5207	—
6 (S)	0	1.3226	1.3115	1.3115	1.3104	1.3104
	$5 \times 10$	0.7197	0.7158	0.7125	0.7121	0.7113

	10×10	0.7140	0.7126	0.7119	0.7115	0.7109
	20×10	0.7127	0.7114	0.7109	0.7108	0.7106
	30×10	0.7126	0.7112	0.7107	0.7106	—

\* (S) symmetric mode in  $\theta$ ; (A) antisymmetric mode in  $\theta$   
 — No results due to matrix ill-conditioning

Table 2. Convergence of frequency parameters  $\Lambda$  for a completely free hexagonal cylindrical solid ( $N=6$ ) having a V-notch ( $\alpha = 355^\circ$ ,  $c/a = 0.75$ ,  $h/l = 2$ )

Mode no. (sym. class *)	Size of edge function	Solution size of polynomials				
		4×10	5×10	6×10	7×10	8×10
1 (A)	0	0.4576	0.4568	0.4568	0.4567	0.4567
	5×10	0.4547	0.4546	0.4545	0.4545	0.4545
	10×10	0.4546	0.4545	0.4545	0.4545	0.4545
	20×10	0.4544	0.4544	0.4544	0.4544	0.4544
	30×10	0.4542	0.4541	0.4541	0.4541	—
2 (A)	0	0.4871	0.4871	0.4759	0.4759	0.4757
	5×10	0.4635	0.4620	0.4619	0.4618	0.4617
	10×10	0.4618	0.4618	0.4618	0.4616	0.4614
	20×10	0.4602	0.4601	0.4600	0.4599	0.4597
	30×10	0.4549	0.4549	0.4549	0.4548	—
3 (S)	0	0.4574	0.4565	0.4565	0.4565	0.4565
	5×10	0.4565	0.4564	0.4564	0.4563	0.4563
	10×10	0.4564	0.4563	0.4563	0.4563	0.4563
	20×10	0.4563	0.4563	0.4563	0.4562	0.4562
	30×10	0.4560	0.4559	0.4559	0.4559	—
4 (S)	0	0.7755	0.7755	0.7755	0.7755	0.7755
	5×10	0.7754	0.7754	0.7754	0.7754	0.7754
	10×10	0.7754	0.7754	0.7754	0.7754	0.7754
	20×10	0.7754	0.7754	0.7754	0.7754	0.7754
	30×10	0.7754	0.7754	0.7754	0.7754	—
5 (A)	0	0.8861	0.8818	0.8818	0.8812	0.8812
	5×10	0.8717	0.8709	0.8706	0.8705	0.8705
	10×10	0.8709	0.8705	0.8705	0.8704	0.8704
	20×10	0.8702	0.8699	0.8698	0.8698	0.8698
	30×10	0.8689	0.8685	0.8685	0.8684	—
6 (S)	0	0.8864	0.8819	0.8818	0.8814	0.8813
	5×10	0.8820	0.8812	0.8812	0.8810	0.8810
	10×10	0.8816	0.8810	0.8809	0.8809	0.8809
	20×10	0.8812	0.8807	0.8806	0.8806	0.8805
	30×10	0.8794	0.8789	0.8789	0.8789	—

\* (S) symmetric mode in  $\theta$ ; (A) antisymmetric mode in  $\theta$   
 — No results due to matrix ill-conditioning

#### 4. FREQUENCY RESULTS AND MODE SHAPES

Extensive convergence studies were performed to compile the least upper bound frequency parameters for the first six modes of the hexagonal cylindrical solid with increasing vertex

angles and with increasing notch depths. Depicted in Fig. 2 are four typical plate configurations which were analyzed to construct the summary of results in Table 3. All frequency results shown in Table 3 are converged to the five significant figures. Hence, Table 3 provides a reasonably accurate database of frequencies for V-notched hexagonal cylinders having various notch angles and depths against which future results using modern experimental or alternative theoretical approaches may be compared.

Table 3. Frequency parameters  $\Lambda$  for a completely free hexagonal cylindrical solid ( $N=6$ ) with V-notches

$\alpha$	$c/a$	Mode					
		1	2	3	4	5	6
90°	0.75	0.3873	0.4129	0.4566	0.7791	0.8193	0.8473
	0.5	0.3483	0.3912	0.4468	0.7672	0.7804	0.8240
	0.0	0.2537	0.3389	0.3999	0.6060	0.7528	0.7826
	-0.5	0.1382	0.2287	0.3334	0.3598	0.5614	0.6555
180°	0.75	0.4260	0.4624	0.4677	0.7763	0.8608	0.8824
	0.5	0.3898	0.4411	0.4661	0.7770	0.8201	0.8737
	0.0	0.2981	0.3627	0.4527	0.6800	0.7228	0.7789
	-0.5	0.1668	0.2744	0.3993	0.4301	0.5587	0.7751
270°	0.75	0.4521	0.4564	0.4630	0.7756	0.8726	0.8802
	0.5	0.4341	0.4378	0.4571	0.7756	0.8547	0.8640
	0.0	0.3463	0.3899	0.4485	0.7180	0.7494	0.7801
	-0.5	0.2234	0.3345	0.3710	0.4082	0.4708	0.6005
300°	0.75	0.4530	0.4554	0.4642	0.7755	0.8722	0.8786
	0.5	0.4302	0.4473	0.4525	0.7752	0.8475	0.8588
	0.0	0.3353	0.4230	0.4305	0.6043	0.6632	0.7179
	-0.5	0.2306	0.2997	0.3621	0.3854	0.3897	0.5824
330°	0.75	0.4543	0.4546	0.4633	0.7755	0.8709	0.8788
	0.5	0.4298	0.4495	0.4522	0.7749	0.8446	0.8596
	0.0	0.3328	0.4173	0.4447	0.4991	0.5672	0.7274
	-0.5	0.2149	0.2333	0.3128	0.3563	0.4406	0.5159
350°	0.75	0.4548	0.4550	0.4553	0.7754	0.8689	0.8786
	0.5	0.4256	0.4471	0.4545	0.7746	0.8418	0.8529
	0.0	0.3353	0.4136	0.4450	0.4610	0.5289	0.7158
	-0.5	0.1849	0.2445	0.2945	0.3626	0.4514	0.5136
355°	0.75	0.4541	0.4548	0.4559	0.7754	0.8684	0.8789
	0.5	0.4254	0.4467	0.4550	0.7745	0.8416	0.8528
	0.0	0.3361	0.4134	0.4391	0.4580	0.5206	0.7105
	-0.5	0.1789	0.2477	0.2913	0.3651	0.4519	0.5154
359°	0.75	0.4536	0.4546	0.4564	0.7754	0.8681	0.8790
	0.5	0.4258	0.4466	0.4553	0.7745	0.8419	0.8537
	0.0	0.3368	0.4132	0.4328	0.4572	0.5140	0.7062
	-0.5	0.1747	0.2502	0.2892	0.3678	0.4514	0.5177
Hexagonal cylinder <sup>+</sup>		0.4564	0.4570	0.4749	0.7755	0.8810	0.8814

\* indicates antisymmetric modes

<sup>+</sup> Results cf. Liew, et al.(1997)

For various  $\alpha$ , some interesting trends can be seen in Table 3 in variation of frequencies as notch depth increases. For instance, for  $\alpha = 330^\circ$ ,  $350^\circ$ , and  $355^\circ$ , the frequencies in the first six modes monotonically decrease with increasing notch depth, except in the fourth and fifth modes for  $\alpha = 330^\circ$  and  $350^\circ$ . Generally speaking, some of frequency trends are quite unpredictable; that is, they sometimes exhibit an increase or decrease with increasing  $\alpha$ , according to the vibration mode. Regardless of the notch angles, the frequency parameters decrease by the notch. As can be known, the hexagonal cylinders  $\alpha = 90^\circ$  (see Fig. 3) and  $180^\circ$  do not form a V-notch, but the frequency data indicate some interesting special case of pentagonal and isosceles triangular cylindrical solids.

It is important at this point to compare the frequency data shown in Table 3 for the case of a sharp shallow crack ( $c/a = 0.75$  and  $\alpha = 359^\circ$ ) with the data for a complete hexagonal cylindrical solid. As seen in Table 4, the crack reduces the frequencies of the symmetric modes 3, 4 and 6 by 3.90%, 0.01% and 0.27%, respectively, and those of the antisymmetric modes, 1, 2, and 5 by 0.61%, 0.53% and 1.46%, respectively. For the of a sharp, deep crack ( $c/a = 0$  and  $\alpha = 359^\circ$ ), the per cent reductions in frequencies of the symmetric modes 3, 4, 5 and 6 are 8.87, 41.04, 41.66 and 19.88 per cent, respectively, and those in the antisymmetric modes 1 and 2 are 26.21 and 9.58 per cent, respectively.

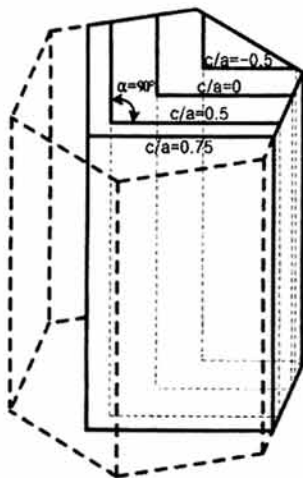


Fig 3. Cylinders with  $90^\circ$  and various depth ratios

Comparisons are made in Figs. 4 and 5 for frequency parameters  $\Lambda$  of hexagonal cylinders with two different notch angles (i.e.,  $\alpha = 270^\circ$  and  $355^\circ$ ), having  $c/a = 0.75, 0$ , and  $-0.5$ . In these graphs the frequency results obtained by the present three-dimensional elasticity-based theory are compared with those produced by using the finite element approach. The finite element solutions were obtained using more than eighty thousand elements of solid45 with eight nodes and modal analysis with block Lancos mode extraction method in ANSYS (2001). Here, very fine mesh generation is used near the terminus edge of the completely free, notched hexagonal cylinder in order to consider the stress singularities. It can be seen in Figs. 4 and 5 that the present three-dimensional theory gives slightly lower  $\Lambda$  values than those of FEM, and also offers favorable agreement between two approaches.

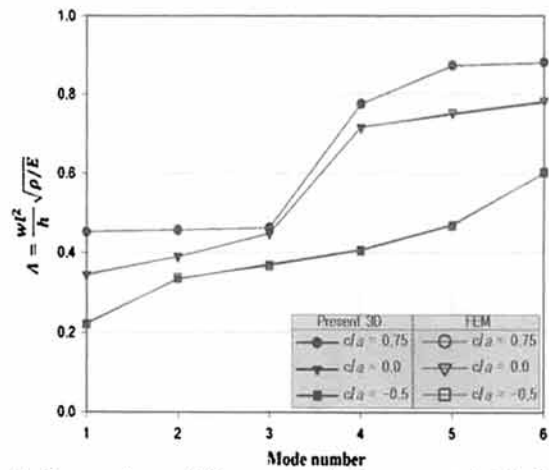


Fig 4. Comparison of frequency  $\Lambda$  for a completely free polygonal cylindrical solids with V-notches ( $\alpha = 270^\circ$ )

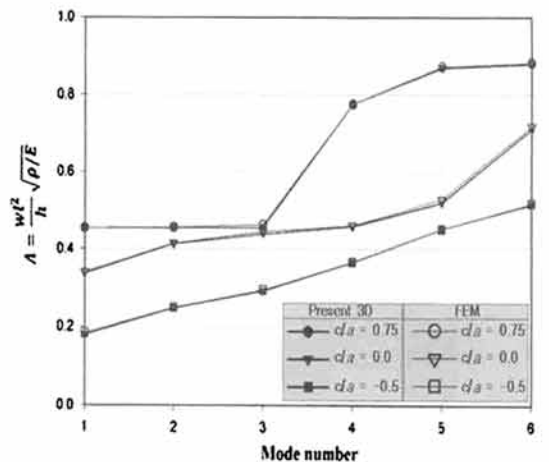

















Fig 5. Comparison of frequency  $\Lambda$  for a completely free polygonal cylindrical solids with V-notches ( $\alpha = 355^\circ$ )

Figs. 6 and 7 depict the deformed mode shape contours of cylindrical solids with hexagonal cross-sections with  $\alpha = 270^\circ$  and  $355^\circ$ , respectively, having  $c/a = 0.75, 0$  and  $-0.5$ . It can be observed from these mode shapes that there are axial extensional, first or second lateral bending and axial torsional motions according to each mode and  $c/a$  ratios. Non-dimensional frequencies shown with the mode shapes correspond to the data listed in Table 3.

Mode No.	$c/a$		
	0.75	0	-0.5
1			
	0.4521	0.3463	0.2234
2			
	0.4564	0.3899	0.3345
3			
	0.4630	0.4485	0.3710
4			
	0.7756	0.7180	0.4082
5			
	0.8726	0.7494	0.4708



















6			
	0.8802	0.7801	0.6005

Fig 6. Vibration mode shapes of hexagonal cylinder with  $\alpha = 270^\circ$  and different depth ratios ( $h/l = 2$ )

Mode No.	$c/a$		
	0.75	0	-0.5
1			
	0.4541	0.3361	0.1789
2			
	0.4548	0.4134	0.2477
3			
	0.4559	0.4391	0.2913
4			
	0.7754	0.4580	0.3651
5			
	0.8684	0.5206	0.4519






6			
	0.8789	0.7105	0.5154

Fig 7. Vibration mode shapes of hexagonal cylinder with  $\alpha = 355^\circ$  and different depth ratios ( $h/l = 2$ )

The effects of varying the number of sides of polygonal cross-section are observed in Table 4, where  $\alpha = 355^\circ$ . According to the number of sides ( $N$ ), they may be considered as the cylindrical solids with octagonal ( $N = 8$ ), decagonal ( $N = 10$ ) and dodecagonal ( $N = 12$ ) cross-sections.

For various number of sides, some interesting trends are shown in Table 4 in the variation of frequency parameters as the notch depth decreases (i.e.,  $c/a$  increases). For  $c/a = 0$ , the fundamental frequencies increase with increasing the number of sides, whereas for  $c/a = 0.75$ , they decrease at increased number of sides. The higher modes sometimes display an increase or a decrease with increasing  $N$ .

For various number of sides, some interesting trends are shown in Table 4 in the variation of frequency parameters as the notch depth decreases (i.e.,  $c/a$  increases). For  $c/a = 0$ , the fundamental frequencies increase with increasing the number of sides, whereas for  $c/a = 0.75$ , they decrease at increased number of sides. The higher modes sometimes display an increase or a decrease with increasing  $N$ .

Table 4. Frequency parameters  $\Lambda$  for a completely free N-sided cylindrical solids with V-notches ( $\alpha = 355^\circ$ )

$c/a$	No. of sides ( $N$ )	Mode No.					
		1	2	3	4	5	6
0	6	0.3361*	0.4134*	0.4391	0.4580	0.5206	0.7105
	8	0.3409*	0.4086*	0.4439	0.4618	0.5338	0.7213
	10	0.3425*	0.4067*	0.4427	0.4667	0.5394	0.7259
	12	0.3434*	0.4056*	0.4417	0.4697	0.5425	0.7285
0.75	6	0.4541*	0.4548*	0.4559	0.7754	0.8684*	0.8789
	8	0.4475*	0.4492*	0.4554*	0.7760	0.8650*	0.8763
	10	0.4446*	0.4478*	0.4602*	0.7762	0.8637*	0.8773
	12	0.4441*	0.4453*	0.4577*	0.7763	0.8633*	0.8749

\* indicates antisymmetric modes

## 5. CONCLUDING REMARKS

Highly accurate frequencies and mode shapes for completely free solid cylinders of N-sided polygonal cross-section with V-notches or cracks have been obtained using a three-dimensional continuum-based Ritz procedure. In this approximate procedure, the assumed displacements of the hexagonal solid constitutes a hybrid set of mathematically complete algebraic-trigonometric polynomials with three-dimensional edge functions that account tri-axial stress singularities along the terminus edge of the V-notch. The efficacy of such edge functions has been substantiated by an convergence study of non-dimensional frequencies.

A detailed numerical table has been presented, showing the variations of non-dimensional frequencies (accurate to five significant figures) with two geometric parameters: namely, notch angles and notch depths. Some fundamental understanding of the effect of highly localized stresses on the notched or cracked cylinder dynamics can be obtained through careful examination of the frequency and mode shape data offered here in.

## ACKNOWLEDGEMENTS

This work was supported by the Korea Research Foundation Grant funded by the Korean Government (KRF-2005-041-D00851).

## REFERENCES

- Timoshenko, S.P., (1921a) On the Correction for Shaer of the Differential Equation for Transverse Vibration of Prismatic Bars, *Philosophical Magazine*, Vol. 41, pp.744-746.
- Timoshenko, S.P., (1921b) On the Transverse Vibration of Bars Uniform Cross-section, *Philosophical Magazine*, Vol. 43, pp. 125-131.
- Kim, J.W., Jung, H.Y., and Kwon I.K., (2001) Three-dimensional Vibration Analysis of Parallelepipeds with V-notches or Sharp Cracks, *Proceedings of IMAC-XIX: A Conference of Structural Dynamics*, Vol. 2, pp.1528-1534.
- Kim, J.W., Jung, H.Y., Lee, D.W. and Lee S.S., (2006) Transverse Vibration of V-notched or Cracked Plates with N-sided Polygonal Boundary Shape, *International Symposium of IASS-APCS*, DR33.

Kim, J.W. and Jung, H.Y., (2007) Accurate Vibration Analysis of  $N$ -sided Polygonal Mindlin Plates with V-notches or Sharp Cracks, *Proceedings of the International Conference on ANDE 2007*, Vol. 2, pp. 1456-1461..

Liew, K.M., Hung, K.C. and Lim, M.K., (1997) Three-dimensional Vibration Analysis of Solid Cylinders of Polygonal Cross-Section Using the

$p$ -Ritz Method, *Journal of Sound and Vibration*,  
Vo. 200, No. 4, pp.505-518.

ANSYS User' Manual, (2001) Release 6.0, ANSYS, Inc.

(접수일자 : 2009. 4. 22 / 심사일 2009. 5. 25 /  
게재확정일 2009. 8. 10)